Design, Synthesis, and Density Functional Theory Studies of Indole Hydrazones as Colorimetric "Naked Eye" Sensors for F Ions

Rima D. Alharthy,* Nadeem Ahmed, Saman Mubarak, Muhammad Yaqub, Muhammad Khalid,* Iqra Shafiq, Muhammad Adnan Asghar, Ataualpa Albert Carmo Braga, and Zahid Shafiq*

ACCESS | Metrics & More | Article Recommendations | Supporting Information

ABSTRACT: A new series of sensors **SM-1** to **SM-3** was designed and synthesized using indole carboxaldehydes (**2a−2c**) and 2,4-dinitrophenyl hydrazine. Accompanied by the synthesis, density functional theory investigation was also accomplished at the M06-2X/6-311G+(d,p) functional. A reduction in band gap (ΔE = 4.702−4.230 eV) along with a bathochromic shift (λ_{max} = 433.223−471.584 nm) was seen in deprotonated chromophores than their neutral sensors. Further, significant charge transference from indole toward dinitrophenyl hydrazine was also examined.

Global reactivity parameters also expressed the greater stability of sensors than that of their deprotonated form. **SM-3** displayed high selectivity toward F ions as compared to **SM-1** and **SM-2**, which respond to both F⁻ and CN⁻ ions. The electronic absorption spectrum was recorded in CH₃CN. The sensor **SM-3** showed high selectivity toward F⁻ ions with a low detection limit (8.69×10^{-8}), and the binding constant for **SM-3** was determined as 7.7×10^5. The sensor displayed naked eye views as the color of solution changed from mustard to purple with a red shift of 96 nm. The mechanism suggests deprotonation from the NH group, which was confirmed by ¹H NMR. The sensor is found to be useful for detection of F⁻ ions in the real sample and for analytical application (test strip).
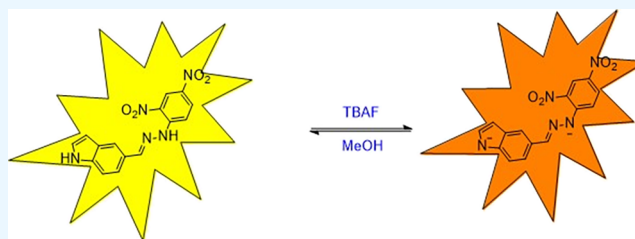
1. INTRODUCTION

Chemosensor schemes catch the substantial interest for monitoring cations and anions, because "guest−host" contact can alter the physical properties, such as fluorescence (fluorogenic sensors) or color (chromogenic sensors).[1] Due to their high compassion, selectivity, and ability to achieve in situ and in vivo investigation, chemosensors are mainly proficient apparatus for distinguishing a variety of analytes. Also, chemosensors have simplicity and ease of understanding and are extensively used for the detection of the ionic composition of the medium in organic chemistry, biology, medicine, and environmental research.[2] Due to their significant function in an extensive range of ecological, medical, chemical, and biological purposes, the identification and sensing of anions have gained noteworthy concentration.[3] Among the anions, fluoride ions (F⁻) have gained much attention. Fluoride is the smallest and most significant electronegative atom having different chemical properties and also forms a strong hydrogen bond with target molecules.[4] F⁻ ions are determined to be valuable to avoid dental caries. Chronic ingestion of fluoride, even though below 1 mg/L, can cause insensitive dental and skeletal fluorosis. Accumulation of F⁻ ions over a period can cause interference with liver and kidney functions, change in the DNA structure, lowering of IQ of children, and loss of mobility.[5] With increasing industries of food products and cosmetic goods of fluorine products, the

infection of fluorine turns out to be more serious. For these reasons, detection of fluoride ions is necessary.

Currently, UV−vis absorption spectroscopy and colorimetric naked-eye detection methods have engrossed extensive concentration because they can be advantageous and inexpensive equipment is required for detection. An anionic chemosensor can yield binding information by both behaviors (fluorescence or absorption spectra).[6] The color differences are connected with structural or conformational changes after the addition of anions to receptors.[7] These routes are based on N−H proton transfer from the receptor to an anion.[8] The receptors involved for donation of protons include urea, amine, imidazole ions, phenol, hydroxyl groups, pyrrole, imine, thiourea, and hydrazones.[9]

Hydrazones of 2,4-dinitrophenyl hydrazines are very useful chemosensors used for the detection of anions, especially fluoride and cyanide ions. There was a strong alteration in color after the addition of anions to these hydrazones. This change was attributed to abstraction of protons from

hydrazones. These hydrazones have strong acidic protons, which form hydrogen bonding with added anions.[10] Herein, a series of novel hydrazones (**SM-1** to **SM-3**) based on the indole carboxaldehyde derivative and 2,4-dinitrophenyl hydrazine moiety was synthesized in a single step. The synthesized compounds respond to F⁻ and CN⁻ ions, except **SM-3**, which displayed high selectivity toward F⁻ ions. We predicted that our synthesized compounds possess acidic protons, which were abstracted by anions (F⁻ and CN⁻), and as a result, fast and sensitive detection was observed.

2. EXPERIMENTAL SECTION

All the chemicals such as indole-4-carboxaldehyde, indole-5-carboxaldehyde, indole-6-carboxaldehyde, 2,4-dinitrophenyl hydrazine (DNPH), MeOH, acetic acid, petroleum ether, salts (tetrabutyl ammonium salts (bisulfate, F, chloride, iodide, bromide, perchlorate, thiocyanate, acetate, and cyanate)), and ethyl acetate were obtained from Sigma-Aldrich. The reaction was carried out in an oven-dried flask (50 mL). The ^{1}H NMR spectrum was recorded on a Bruker MHz 400 spectrometer. The electronic absorption spectra were recorded on a Shimadzu UV-1800 spectrophotometer.

2.1. Computational Procedure. In the current study, quantum chemical investigation was performed for **SM-1** to **SM-3** sensors and their ionic forms: **an1** (formed by deprotonation from the −N=NH group), **an2** (formed by deprotonation from the indole group), and **an3** (formed by double deprotonation from the −N=NH group and indole group). For this purpose, the Gaussian 09 package[11] was utilized at the M06-2X/6-311G+(d,p) functional[12] of density functional theory (DFT) in acetonitrile. Frontier molecular orbital analysis was performed to elucidate the charge transference and energy gap between the orbitals. From the findings of FMOs, global reactivity parameters were investigated to understand the reactivity and stability of these sensors. To investigate the excitations of sensors, UV−vis, hole−electron, and transition density matrix (TDM) analyses were also performed in acetonitrile media at the foresaid functional.

2.2. Synthesis of Chemosensors. The chemosensors were synthesized *via* a single-step condensation reaction of the indole-carboxaldehyde (0.1 g, 0.30 mmol) derivative with 2, 4-dinitrophenyl hydrazine (0.1 g, 0.30 mmol) in MeOH (15 mL) (Scheme 1). The reaction was refluxed at 70 °C and initiated by the addition of a catalyst (CH₃COOH). After some time, precipitates were formed. The reaction was monitored by TLC and, after the completion of reaction, confirmed by TLC. The precipitates were filtered, washed with MeOH, and dried in air. The yield was calculated as 80%. The synthesized compounds were confirmed by the ^{1}H NMR and ^{13}C NMR spectra (Figures S1−S6). The reaction was monitored by TLC.

SM-1: (*E*)-4-((2-(2,4-dinitrophenyl)hydrazono)methyl)-1*H*-indole. m.p.: >300 °C. IR v_{max} (cm⁻¹): 1175 (C=S), 1570 (C=N), 3125, 3311 (N−H); ^{1}H NMR (DMSO-d_6) δ (ppm): 11.60 (1 H, s), 11.35 (1 H, s), 8.81 (2 H, d, *J* = 62.4), 8.38 (1 H, d, *J* = 7.7), 8.08 (1 H, d, *J* = 8.2), 7.75 (1 H, s), 7.62 (1 H, d, *J* = 6.5), 7.52 (2 H, d, *J* = 34.8), 6.49 (1 H, s). ^{13}C NMR δ (ppm): 101.91, 112.31, 116.75, 117.88, 120.69, 123.29, 126.82, 128.18, 129.14, 129.92, 135.91, 136.72; elemental analysis calculated for C₁₅H₁₁N₅O₄, 325.08; C, 55.39; H, 3.41; N, 21.53; found: C, 55.59; H, 3.19; N, 21.61.

SM-2: (*Z*)-5-((2-(2,4-dinitrophenyl)hydrazono)methyl)-1*H*-indole. m.p.: >300 °C. IR v_{max} (cm⁻¹): 1188 (C=S),

Scheme 1. Synthesis of Indole-Based Sensors (SM-1 to SM-3)
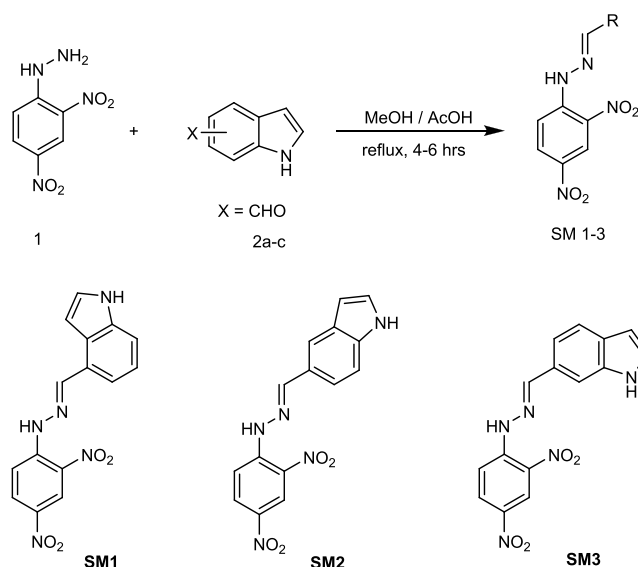
1581 (C=N), 3129, 3323 (N−H); ^{1}H NMR (DMSO-d_6) δ (ppm): 11.57 (1 H, s), 11.36 (1 H, s), 8.78 (2 H, d, *J* = 62.4), 8.34 (1 H, s), 8.08 (1 H, s), 7.89 (1 H, s), 7.64 (1 H, s), 7.44 (2 H, d, *J* = 36.4), 6.53 (1 H, s). ^{13}C NMR δ (ppm): 102.26, 112.30, 116.79, 119.85, 121.79, 123.25, 125.03, 126.83, 127.88, 128.96, 129.82, 136.58, 137.47, 141.63, 151.97; C₁₅H₁₁N₅O₄, 325.08; C, 55.39; H, 3.41; N, 21.53; found: C, 55.51; H, 3.35; N, 21.71.

SM-3: (*Z*)-6-((2-(2, 4-dinitrophenyl)hydrazono)methyl)-1*H*-indole. m.p.: >320 °C. IR v_{max} (cm⁻¹): 1158 (C=S), 1579 (C=N), 3139, 3311 (N−H); ^{1}H NMR (DMSO-d_6) δ (ppm): 11.64 (1 H, s), 11.44 (1 H, s), 8.95 (1 H, s), 8.85 (1 H, s), 8.42 (1 H, d, *J* = 8.9), 8.05 (1 H, d, *J* = 9.1), 7.54 (2 H, s), 7.34 (1 H, d, *J* = 6.4), 7.19 (1 H, t, *J* = 6.8), 7.07 (1 H, s). ^{13}C NMR δ (ppm): 101.93, 114.63, 116.57, 121.01, 122.45, 123.25, 124.62, 124.85, 127.46, 129.24, 130.16, 136.55, 136.82, 144.53, 151.74; C₁₅H₁₁N₅O₄, 325.08; C, 55.39; H, 3.41; N, 21.53; found: C, 55.49; H, 3.35; N, 21.55.

3. RESULTS AND DISCUSSION

3.1. Solvatochromic Behavioral Studies of SM-3. To evaluate the solvatochromic effect, the UV−vis spectrum of **SM-3** with F⁻ ions in different solvents was recorded. The addition of 3 equiv of F⁻ ions to the sensor **SM-3** displayed changes in absorbance band, and the change in wavelength is negligible; thus, there is no effect of polarities of solvents on the sensor **SM-3**, except DCM and CH₃Cl, as illustrated in Figure 1. We have used MeCN as a solvent for next further study.

3.2. Anion Tracking Study. The anion tracking ability of sensors **SM-1** to **SM-3** was checked by the naked-eye view after the addition of different anions such as F⁻, CN⁻, SCN⁻, Br⁻, Cl⁻, I⁻, HSO₄⁻², and ClO₄⁻ ions in CH₃CN to the solution of sensors. Interestingly, the color of solutions **SM-1** and **SM-2** was changed from mustard to purple after the addition of F⁻ and CN⁻ ions. But, in the case of **SM-3**, the change was only observed with F ions as depicted in Figure 2. This study showed that the sensor **SM-3** displayed high selectivity as compared to the other two sensors. We have also used NaF as a source of F ions and MeCN/water as a solvent
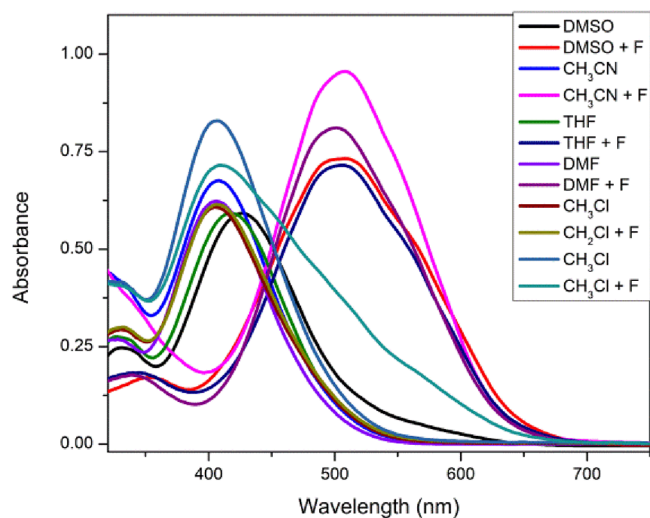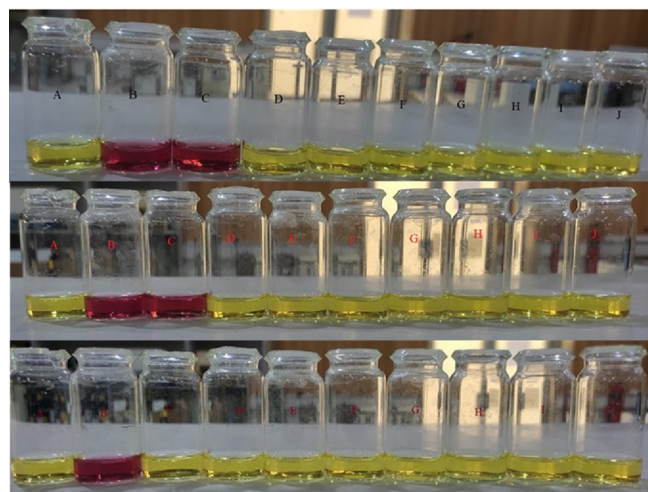
Figure 1. Effect of the solvent on absorbance.

Figure 2. Naked-eye views of sensors **SM-1** to **SM-3** in the presence of 3 equiv of different anions in CH_3CN (A = SM, B = F^-, and C = CN^-).

for the detection of F ions by using **SM-3**, as water has a strong ability to donate its proton as compared to our synthesized sensor **SM-3**. The results are not satisfactory as shown in Figures S7−S9. For further confirmation of selectivity, the UV−vis selectivity of sensors was determined in CH_3CN.

When the solution of sensors was treated with different anions as depicted in Figure 3, there was a change in absorbance band with the addition of F^- and CN^- ions in the case of **SM-1** and **SM-2**. But, in the case of **SM-3**, only the change was observed with F^- ions. This result showed that **SM-3** has high selectivity of detection of F^- ions. This result also supports the naked-eye view results. These changes were attributed to the deprotonation of sensors or the formation of hydrogen bonding with anions and sensors. Due to the high selectivity of **SM-3**, further study was done on it.

3.3. UV−vis Titration with TBAF. To check the ability of anion binding affinity of a sensor with F^- ions, UV−vis titration was carried out. UV−vis titration was performed in CH_3CN as shown in Figure 4. The sensor itself displayed an absorption band at 406 nm in the absence of F^- ions. As addition of F^- ions was continued (0 to 3 equiv), a new
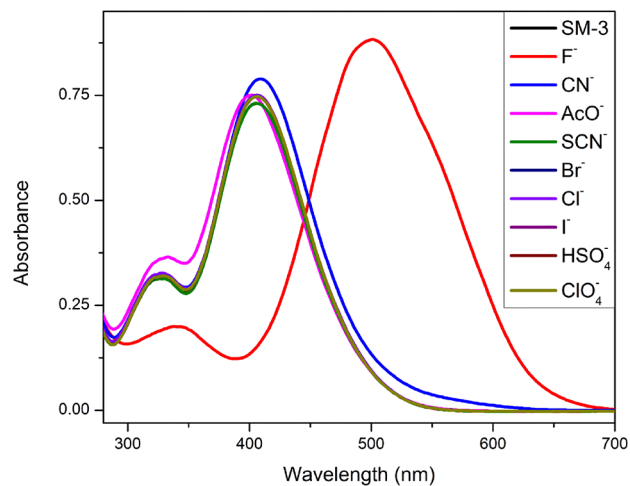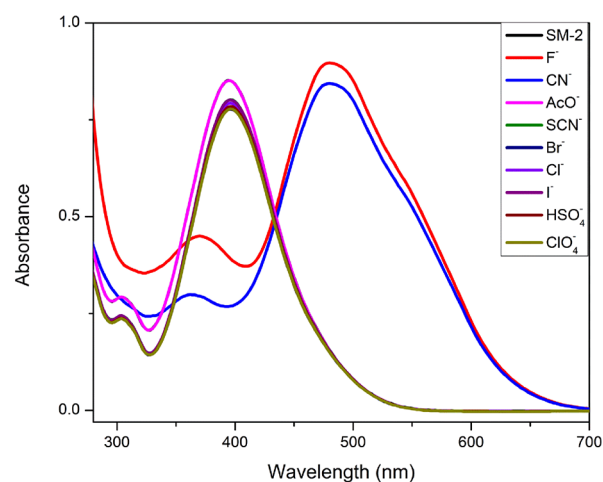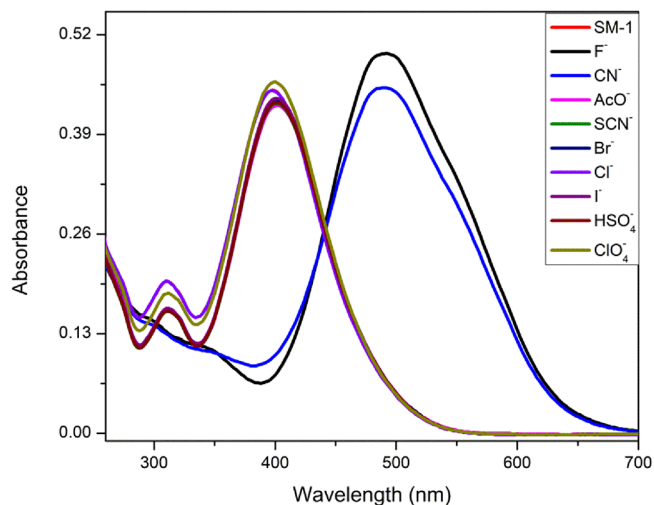

**Figure 3.** UV−vis spectrum of sensors **SM-1** to **SM-3** in CH_3CN.

absorption band at 502 nm was observed with gradual enhancement in absorbance intensity along with a decrease in absorbance intensity at 406 nm. There was a red shift of 96 nm. The appearance of a single isosbestic point at 447 nm was an indication of stable complex formation. The decrease in absorbance band at 406 nm was an indication of deprotonation, which results in a change in color. Job plots indicate that the formation of a complex involved 1:1 stoichiometry (Figure S10). The stoichiometric ratio of the binding of a sensor with
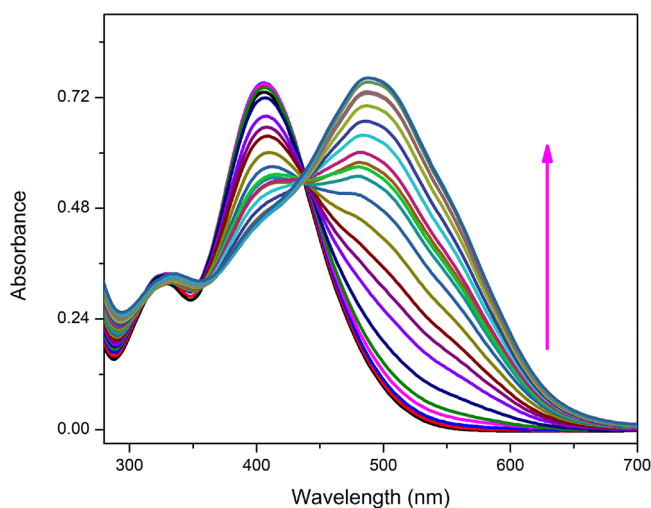
Figure 4. UV−vis titration spectrum of the sensor **SM-3** in CH$_3$CN with 3 equiv of F$^-$ ions.

F$^-$ was calculated by the Benesi−Hildebrand (B−H) plot. The binding constant was calculated as 7.7×10^5, and the detection limit was given as 8.69×10^{-8} (Figures S11 and S12).

3.4. Competitive Study. From above results, it is noted that the F$^-$ ion has a high ability of forming hydrogen bonding/abstracting protons from the sensor **SM-3**. For further confirmation of this statement of high selectivity of F$^-$ ions, a competitive experiment was performed as illustrated in Figure 5. The solution of anions and **SM-3** was treated with
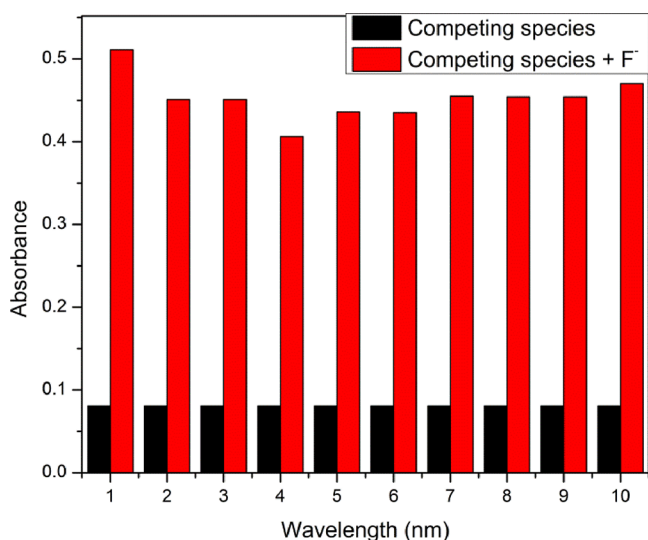
Figure 5. Competitive spectrum of the sensor **SM-3** in CH$_3$CN.

3 equiv of fluoride ions, and it was noted that the competing anions have a negligible effect on the ability of F$^-$ ions to form hydrogen bonding/abstract protons from the sensor **SM-3**. This result showed that **SM-3** has excellent selectivity toward F$^-$ ions.

3.5. Reverse Reaction. One interesting thing is the reversibility of the action of F$^-$ ions with the help of a good proton donor such as methanol.[13] Methanol has the ability to donate protons easily as compared to our synthesized sensor **SM-3**. This statement is justified in Figure 6 as **SM-3** has an absorbance band at 406 nm, which disappeared, and a new
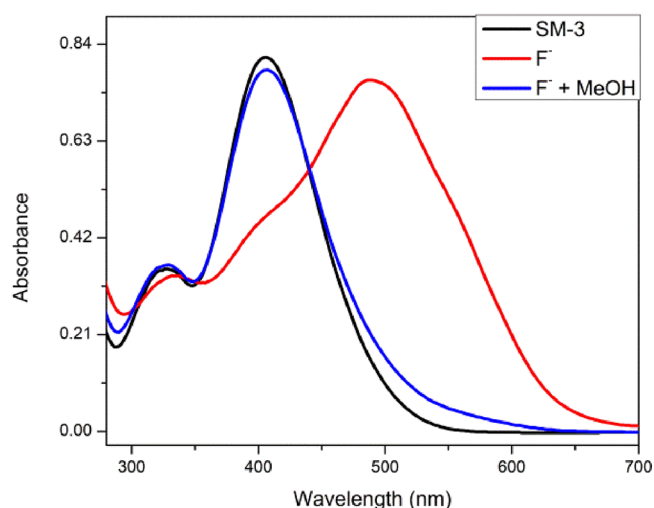

Figure 6. Reverse reaction of **SM-3** with MeOH.

band appeared at 502 nm after the addition of F$^-$ ions. When 0.1 mL of MeOH was added to this complex of **SM-3** and F$^-$ ions, the band that appeared at 502 nm decreased and the original band of **SM-3** reappeared at 406 nm. This showed that **SM-3** displayed a reverse reaction upon addition of MeOH. We have to also try water as well as acids (HCl and acetic acid). The results showed that these solvents are easily deprotonated as compared to our synthesized sensors and a reverse response was observed after the addition of these solvents to the solution of complex of **SM-3** and F$^-$ ions (Figure S13). To support our statement, we have to try other solvents such as ethyl acetate, DMSO, THF, DMF, and EtOH. We have noticed that only change was observed with EtOH (Figure S14). These results showed that solvents that have a strong ability to donate protons as compared to our synthesized sensor can reverse the action of the sensor **SM-3**.

3.6. ^{1}H NMR Titration. To confirm the binding interaction of **SM-3** and F$^-$ ions, a ^{1}H NMR titration experiment was recorded in DMSO-d_6. The ^{1}H NMR spectra of **SM-3** displayed sharp peaks of proton at 11.44 and 11.64 ppm, which were related to N−H and the indole ring, respectively. When a solution of TBAF was added to this solution, the peaks at 11.44 and 11.64 ppm disappeared as illustrated in Figure 7, which confirms the abstraction of protons.
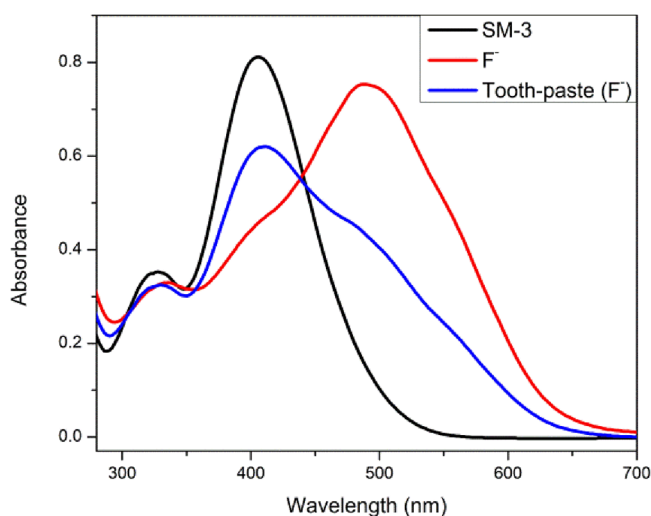

Proposed Sensing Mechanism
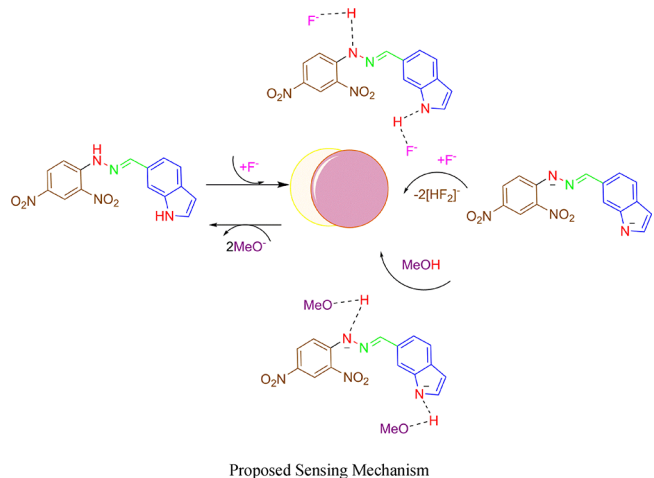
3.7. Real-Life Application. The application of the sensor **SM-3** was demonstrated in real samples like toothpaste. As
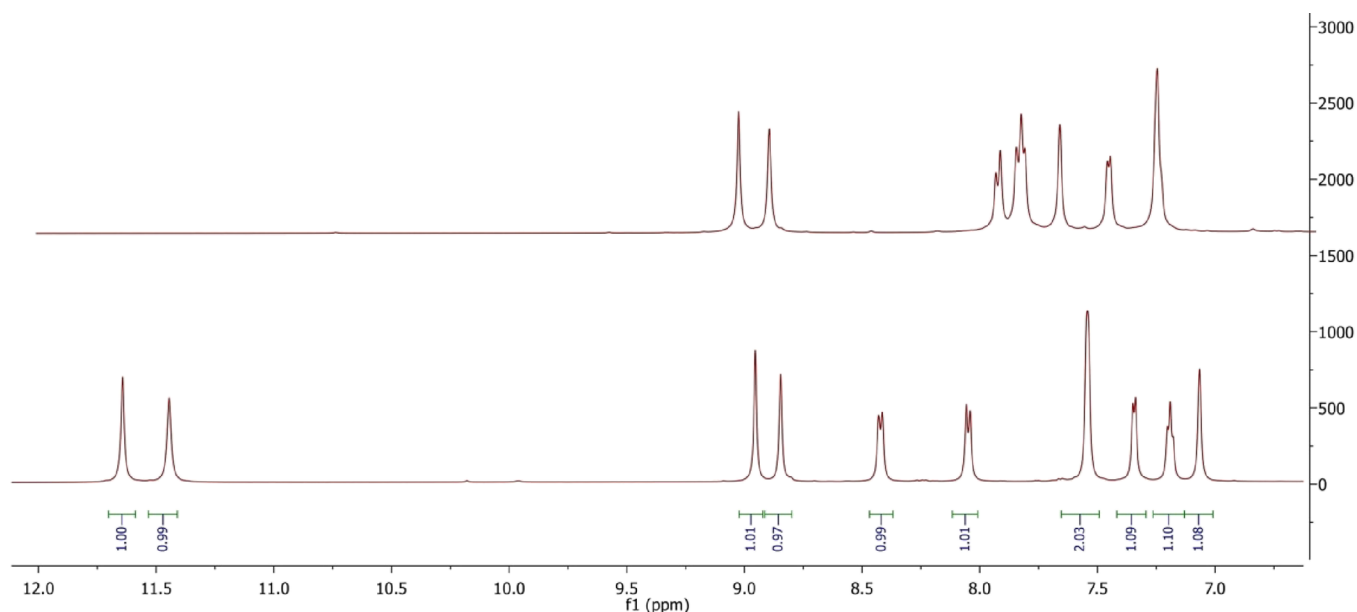
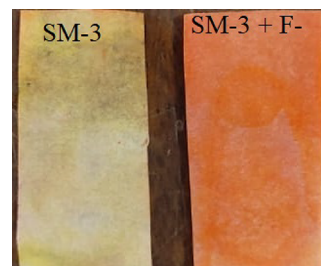**Figure 7.** ^{1}H NMR titration of **SM-3** with and without TBAF.

reported,[14] the toothpaste solution was prepared. When the solution of **SM-3** was treated with the prepared solution of toothpaste, the absorbance band at 406 nm was decreased to some extent and a new band at 502 nm was observed as illustrated in Figure 8. Similarly, to fluoride ions, the color of

Figure 9. Test strip of the sensor **SM-3** for F ion detection.

Figure 8. Treatment of **SM-3** with the toothpaste sample.

solution is also changed from light yellow to purple. These results demonstrate that **SM-3** could be used to detect F$^-$ ions in the toothpaste sample.
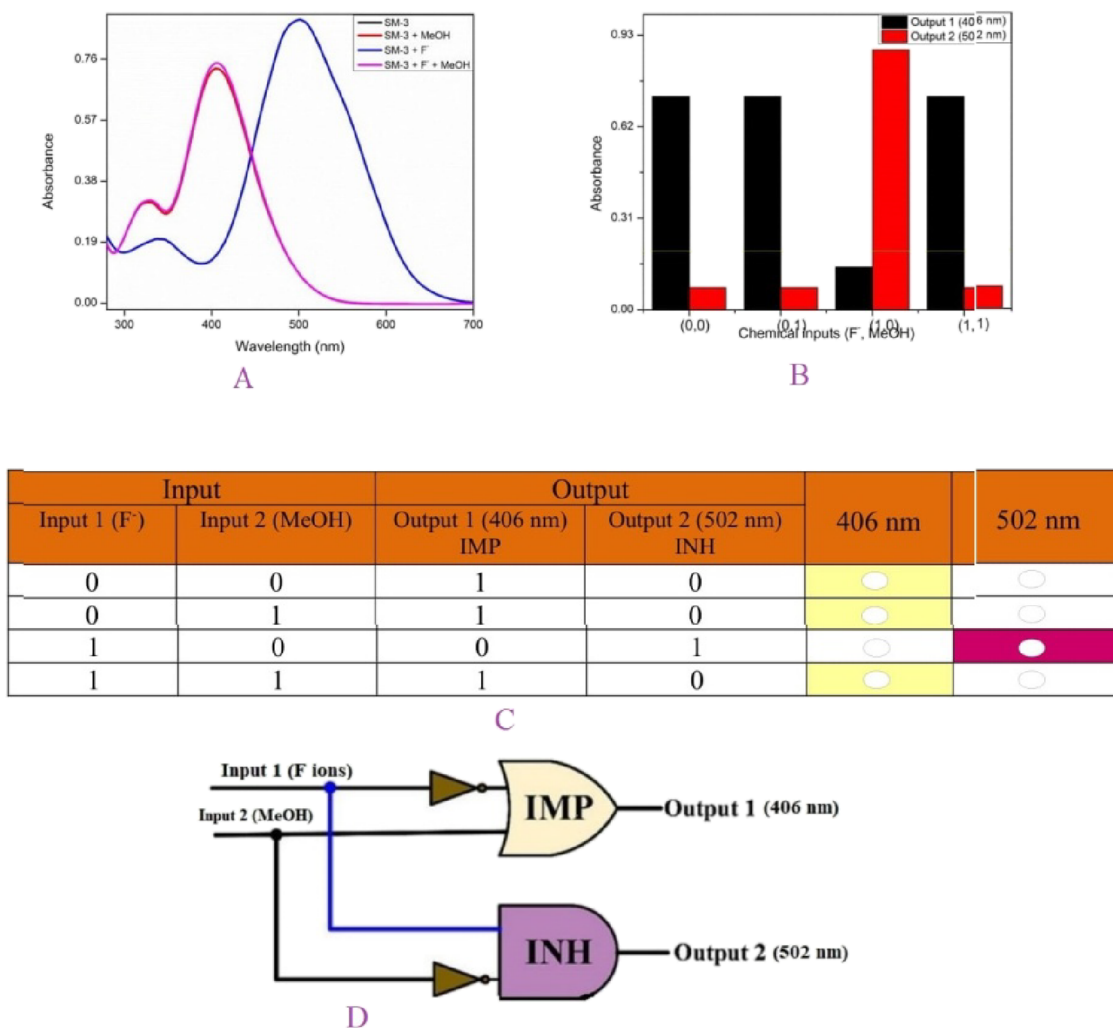
Furthermore, **SM-3** can be used for analytical applications such as test strips. The Whatman filter paper is cut into the form of a test strip (two strips). First, these strips were dipped into the solution of **SM-3**. After that, these strips were air-dried. When these strips were fully dried, one of them was dipped into the solution of F$^-$ ions. The strip color changed from light yellow to peach as shown in Figure 9. This result shows that a test strip can be prepared for F ion detection by using **SM-3**.

3.8. Logic Gate. For the logic gate, F$^-$ ions and MeOH were used as chemical input (1 and 2), while absorbance at 406 and 502 nm was used as chemical output (1 and 2). Binary codes "0" and "1" were used to confirm the presence of chemical inputs. The absorbance valve of 0.2 was used as the threshold valve for 406 and 502 nm. The absorbance valve below the 0.2 valve is given as "0", and the absorbance valve higher than the 0.20 valve is given as "1". This is connected to "off" and "on" positions. As illustrated in Figure 10, in the absence of F ions and MeOH (0, 0) or in the presence of MeOH (0, 1), output 2 (502 nm) is "0", which represents the "off" state. But when input 1 (F$^-$ ions) is present and input 2 (MeOH) is absent, there is a strong absorbance at 502 nm, which shows that output 2 is "1", representing the "on" position. This fabricates an INH gate at 502 nm. Similarly, an IMP gate was constructed, and in the absence of F$^-$ ions and MeOH (0, 0) or in the presence of MeOH (0, 1), the output 1 (406 nm) is "1", which represents the "on" state. But when input 1 (F$^-$ ions) is present and input 2 (MeOH) is absent, the absorbance at 406 nm is quenched, which shows that output 1 is "0", representing the "off" position. Similarly, in the presence of input 1 and input 2, the absorbance band at 406 nm is regained (output 1 is "1"), which represents the "on" state. The IMP logic function output is just complementary to INH logic. These results indicate that the sensor **SM-3** has potential application in molecular devices.

3.9. Frontier Molecular Orbitals (FMOs). The FMO investigation is a valuable tool to understand the reactivity,
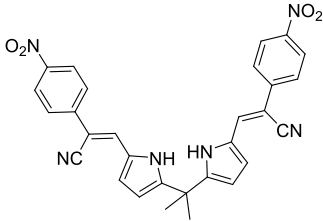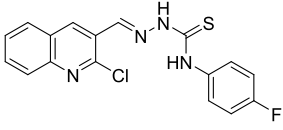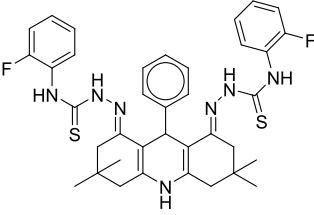
A

B

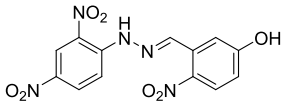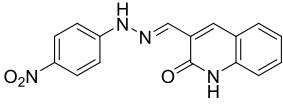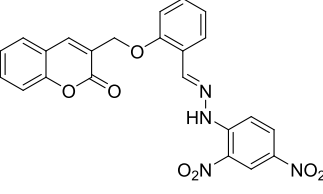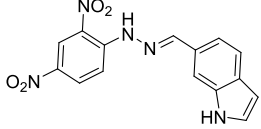| Input		Output		406 nm	502 nm
Input 1 (F⁻)	Input 2 (MeOH)	Output 1 (406 nm) IMP	Output 2 (502 nm) INH		
0	0	1	0	○	○
0	1	1	0	○	○
1	0	0	1	○	●
1	1	1	0	○	○

C

D

Figure 10. (A) Output signal of different inputs, (B) absorbance outcome at different chemical inputs, (C) truth table, and (D) representation of the MP/INH logic circuit.

polarizability, and stability of a molecule.[19] FMO is a powerful factor for determining the possibility of charge transfer among the compounds being studied.[20] The FMO energy gap (E_{gap} = E_{LUMO} − E_{HOMO}) is a representative signature to gain information about charge distribution and ICT rate between molecular orbitals.[14,21] Herein, to investigate the energy gap and charge distribution between orbitals in **SM-1** to **SM-3** sensors and their ions, an FMO study was accomplished, and results are tabulated in Table 2.

The data tabulated in Table 1 shows that the energy gaps of sensors **SM-1**, **SM-2**, and **SM-3** are noted as 4.977, 5.113, and 5.004 eV with HOMO/LUMO energies of −6.889/−1.912, −6.999/−1.886, and −6.899/−1.895 eV, respectively. Among all the studied chemosensors, the highest band gap is seen for **SM-2**, which indicated its higher stability than that of the other sensors. This might be due to the attachment of the 1*H*-indole group at the *meta*-position, which inhibits the charge transference from indole toward the other part of the molecule. The lowest band gap is examined in **SM-1** as the 1*H*-indole group is attached at the *ortho*-position and improves the ICT all over the molecule. As alkyl groups are *ortho*- and *para*-directed by hyperconjugation, the nitrogen (−N) atoms push the electrons into the ring, which increases the electronic density at *ortho*- and *para*-positions due to hyperconjugation.[22]

The overall descending order of band gaps in studied chemosensors is noticed as follows: **SM-2** > **SM-3** > **SM-1**. The comparative study of foresaid chemosensors is done with their respective ions (**an1** to **an3**), and a relative reduction in band gap is noted in ions as compared to their neutral structures (see Table 1). Interestingly, among all ions, greater diminishing is examined in **an2**, which is formed because of the deprotonation from the indole group. Nevertheless, among ions of all sensors, the lowest energy gap is found in **SM-1-an2** (4.230 eV), which indicated its greater reactivity and higher response toward fluoride ions. Overall, the LUMO-HOMO band gap has the following descending order: **SM-3-an1** > **SM-3-an3** > **SM-3-an2**. From abovementioned results, it is concluded that deprotonation from indole facilitates the charge transference, hence resulting in the lowest band gaps of the sensors and improving sensing toward anions. The pictographic representation charge distribution of foresaid sensors along with their ions is illustrated in Figure 11. The charge density for HOMO is majorly concentrated over the indole part and minorly over the 1-(2,4-dinitrophenyl)-2-methylenehydrazine part of sensors. However, for LUMO, the major portion of the electronic cloud is located on 1-(2,4-dinitrophenyl)-2-methylenehydrazine and lower density is seen over the indole unit. These electronic pictures indicate the

Table 1. Evaluation of Limits of Detection and Binding Constants of the Sensor SM-3 with Other Reported Sensors[13a,14−18]

References	Structure	Limit of detection (LOD)	Binding constant (Ka) M⁻
15		20.5×10^{-6}	1.93×10^4
14		9.60×10^{-6}	1.53×10^4
16		9.08×10^{-5}	4.48×10^3
17		2.38×10^{-5}	1.5×10^2
18		1.4×10^{-6}	3.3×10^4
13a		1.1×10^{-6}	1.61×10^4
This work		8.69×10^{-8}	7.7×10^5

excellent charge transference from indole toward the higher electron acceptor region (1-(2,4-dinitrophenyl)-2-methylene-hydrazine). A similar pattern is seen for **an2**. However, in the case of **an1** and **an3**, the charge density for HOMO is concentrated over the entire molecule, whereas, for LUMO, the electronic charge is located on the 1-(2, 4-dinitrophenyl)-2-methylenehydrazine part of the sensor (see Figure 11). The charge transfer in higher orbitals and their energies were also investigated, and their outcomes are described in Figure S15. Almost the same trend for energies and charge

transference is seen in HOMO−1/LUMO+1 and HOMO−2/LUMO+2.

3.10. Global Reactivity Parameters (GRPs). HOMO/LUMO energies are additionally employed to elucidate the reactivity as well as stability of the investigated systems by estimating the global reactivity parameters.[23] The outcome of FMOs (E_{gap}) is a dynamic aspect to calculate the GRPs like ionization potential (IP), electron affinity (EA), electronegativity (X), chemical potential (μ), hardness (η), electrophilicity index (ω), and softness (σ).[24] GRPs for studied

Table 2. E_{HOMO}, E_{LUMO}, and Energy Gap ($E_{LUMO} - E_{HOMO}$) of Investigated Sensors and Their Ionic Forms[a]

| comp.	HOMO	LUMO	energy gap
SM-1	−6.889	−1.912	4.977
SM-1-an1	−6.030	−1.371	4.659
SM-1-an2	−6.064	−1.834	4.230
SM-1-an3	−5.723	−1.403	4.320
SM-2	−6.999	−1.886	5.113
SM-2-an1	−6.092	−1.390	4.702
SM-2-an2	−6.172	−1.820	4.352
SM-2-an3	−5.707	−1.250	4.457
SM-3	−6.899	−1.895	5.004
SM-3-an1	−6.009	−1.330	4.679
SM-3-an2	−6.101	−1.820	4.281
SM-3-an3	−5.646	−1.248	4.398

[a]Units in eV.

sensors were calculated at the M06-2X level of DFT by utilizing eqs S1−S7,[25] and results are shown in Table 3.

Electronegativity, global hardness, and softness are the important qualitative chemical concepts and are extensively utilized to comprehend the different aspects of chemical reactivity. Results of Table 2 reveal that the global softness value is 0.201 eV for SM-1, which is the highest as compared to SM-2 and SM-3. This might be because of the attachment of 2-(2,4-dinitrophenyl)hydrazono)methyl at the *ortho*-posi-

tion of the indole group. The nitrogen (−N) atom pushes the electrons into the ring, which increases the electronic density at −*o* and −*p*-positions due to hyperconjugation. Further, hardness values are found to be 2.489, 2.557, and 2.502 eV for SM-1, SM-2, and SM-3, respectively, and the lowest value of hardness shows that SM-1 is a kinetically least stable, more reactive, and soft chemosensor. Moreover, it can also be inferred from Table 2 that increased values of electronegativity (X) and decreased values of chemical potential (μ) are found for all the ionic forms as compared to their sensors (SM-1, SM-2, and SM-3). Furthermore, in ionic form, the higher softness is noticed for the an2 form as it is formed by the deprotonation from the indole group. It means that deprotonation from indole enhanced the sensing toward fluorides.

3.11. UV−Visible Analysis. To calculate the ground-state electronic transitions in SM-1 to SM-3 sensors, UV−vis investigation was performed *via* time-dependent density functional theory (TD-DFT). The UV−visible absorption spectra of foresaid sensors were simulated in acetonitrile solvent by utilizing the M062x/6-311+G(d,p) functional, and important results are tabulated in Table 4.

Data tabulated in the above table elucidates that the λ_{max} values of sensors SM-1, SM-2, and SM-3 are observed as 401.049, 391.599, and 394.352 nm with transition energies of 3.092, 3.166, and 3.144 eV, respectively. Among all the chemosensors, the maximum absorbance is shown by SM-1
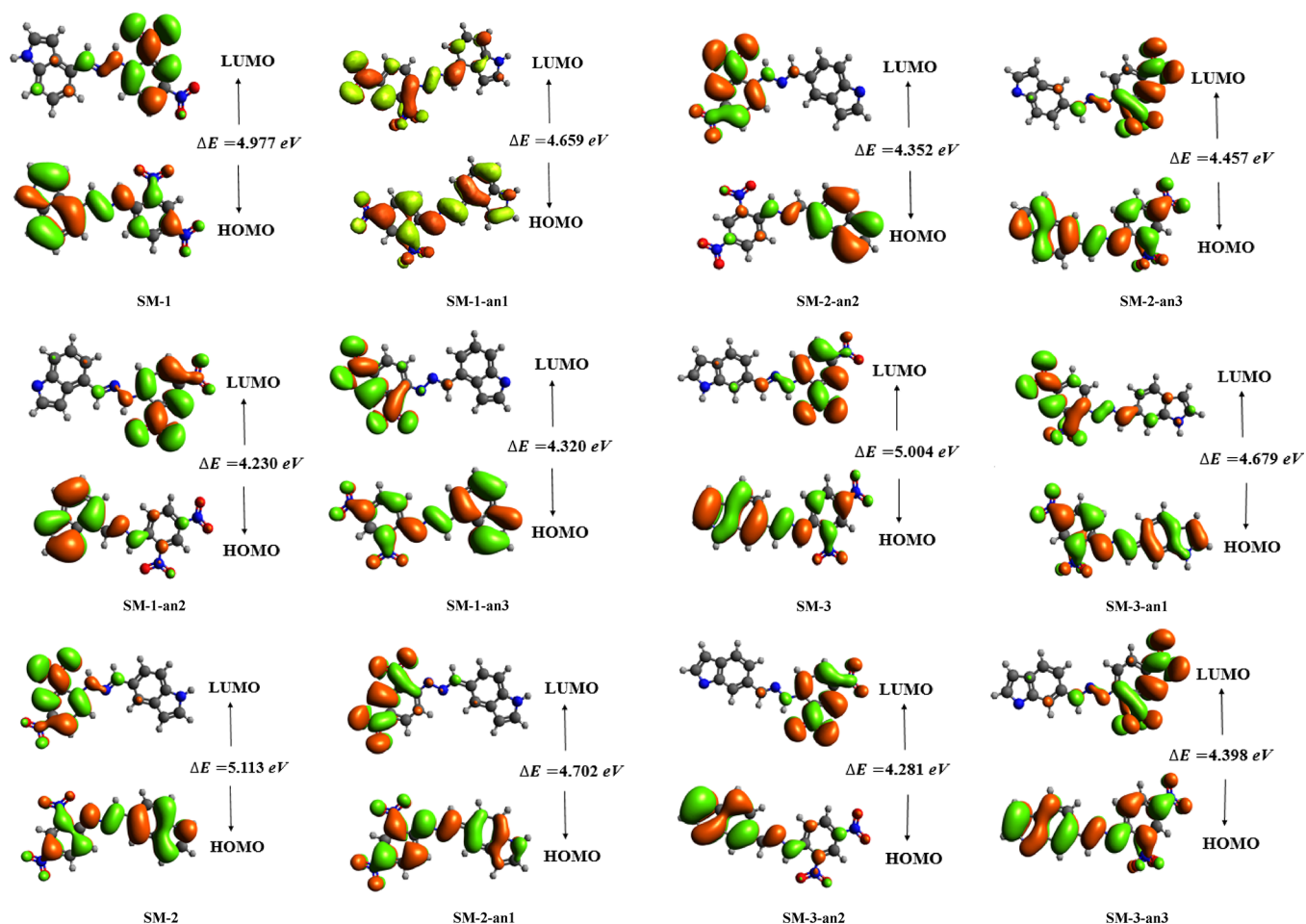
Figure 11. Pictographic charge distribution representation of the HOMO/LUMO orbital of investigated sensors.

Table 3. GRPs of Studied Sensors and Their Respective Ions[a]

compound	IP	EA	X	μ	η	ω	σ
SM-1	6.889	1.912	4.401	−4.401	2.489	3.891	0.201
SM-1-an1	6.03	1.371	3.700	−3.700	2.330	2.939	0.215
SM-1-an2	6.064	1.834	3.949	−3.949	2.115	3.687	0.236
SM-1-an3	5.723	1.403	3.563	−3.563	2.160	2.939	0.231
SM-2	6.999	1.886	4.443	−4.443	2.557	3.860	0.196
SM-2-an1	6.092	1.390	3.741	−3.741	2.351	2.977	0.213
SM-2-an2	6.172	1.820	3.996	−3.996	2.176	3.670	0.230
SM-2-an3	5.707	1.250	3.479	−3.479	2.229	2.715	0.224
SM-3	6.899	1.895	4.397	−4.397	2.502	3.864	0.199
SM-3-an1	6.009	1.330	3.670	−3.670	2.340	2.878	0.214
SM-3-an2	6.101	1.820	3.961	−3.961	2.141	3.664	0.234
SM-3-an3	5.646	1.248	3.447	−3.447	2.199	2.702	0.227

[a]Units in eV.

Table 4. Calculated Transition Energies (eV), Maximum Absorption Wavelengths (λ_{max}), Oscillator Strengths (f_{os}), and Transition Nature of Designed Compounds (SM-1 to SM-3) in Acetonitrile[a]

compound	λ (nm)	E (eV)	f_{os}	MO contributions
SM-1	401.049	3.092	0.975	H → L (61%), H → L + 1 (17%)
SM-1-an1	457.267	2.711	1.546	H → L (81%), H → L + 1 (12%)
SM-1-an2	461.319	2.688	0.766	H → L (38%), H → L + 1 (37%), H → L + 2 (16)
SM-1-an3	471.584	2.629	1.303	H-1 → L (11%), H → L (69%), H → L + 1 (11%)
SM-2	391.599	3.166	0.785	H → L (63%), H → L + 1 (16%), H-2 → L (8)
SM-2-an1	452.002	2.743	0.346	H → L (87%), H-3 → L (2)
SM-2-an2	433.223	2.862	0.816	H-1 → L (15%), H → L (33%), H → L + 1 (25)
SM-2-an3	470.957	2.633	0.391	H → L (73%), H-2 → L (7)
SM-3	394.352	3.144	0.957	H-2 → L (10%), H → L (61%), H → L + 1 (16%)
SM-3-an1	451.130	2.748	0.705	H → L (81%), H-1 → L (3%), H → L + 1 (9)
SM-3-an2	439.084	2.824	0.956	H → L (45%), H → L + 1 (29%), H-2 → L (9%)
SM-3-an3	471.226	2.631	0.439	H → L (70%), H-2 → L (6%), H-1 → L (9%)

[a]MO = molecular orbital; f_{os} = oscillator strength; H = HOMO; L = LUMO.

(401.049 nm) with the lowest energy gap (3.092 eV) and oscillator strength (0.975). This might be due to the attachment of the 1*H*-indole group at the *ortho*-position, which improves the ICT all over the sensor. Overall, the descending order of λ_{max} is **SM-1 > SM-3 > SM-2**.

Comprehensive analysis of abovementioned chemosensors is done with their respective ions (**an1** to **an3**), and the λ_{max} is found to be red-shifted compared to the neutral sensors (see Table 3). For example, in the **SM-1** sensor, the λ_{max} shift values are found as 457.267, 461.319, and 471.584 nm with low energy (2.688 and 2.629 eV) and f_{os} (0.766 and 1.303) values. Correspondingly, the λ_{max} values for **SM-2** ions are estimated to be 433, 452, and 470 nm for **SM-2-an2**, **SM-2-an1**, and **SM-2-an3**, respectively. Similarly, **SM-3-an3**, **SM-3-an1**, and **SM-3-an2** have λ_{max} in decreasing order as 471, 451.130, and 439 nm, respectively. In all sensors, the maximum bathochromic shift is examined in ions when double deprotonation is done (**an3**). Overall, the decreasing order of λ_{max} is **SM-1-an3 > SM-3-an3 > SM-2-an3 > SM-1-an2 > SM-2-an1 > SM-3-an1 > SM-3-an2 > SM-2-an2 > SM-1 > SM-3 > SM-2**. These simulated values of **SM-1** to **SM-3** showed agreement with experimental absorption values (see Figure 3), and among all sensors, **SM-3** and its ions displayed a red shift, so they would express good sensing toward fluoride ions.

3.12. Hole−Electron Analysis. The hole−electron investigation demonstrates almost similar index values for the investigated sensors and their ions as shown in Table 5. From Table 5, compounds **SM-2** and **SM-3** possess high *D* index values at 1.95 and 2.10 Å, respectively, but **SM-1** possesses a medium *D* index value of 1.82 Å, which implies that $S_0 \rightarrow S_1$ excitations involve a medium distance between hole and electron distribution in **SM-1** and a consequently medium E_{Coul} value of 2.47 eV, which does not show a strong hole−electron interaction. However, in the comparative analysis of these chemosensors with the ions, the *D* index values of the ions are greater than their neutral counterparts except for **SM-1-an1** and **SM-3-an1**, which exhibit less values at 0.932 and 2.04 Å, respectively. **SM-2** has manifested a high E_{Coul} value of

Table 5. Indices of Hole−Electron Study Having the Highest f_{os} of Compounds for $S_0 \rightarrow S_1$ Excitation

| compound	SM-1	SM-1-an1	SM-1-an2	SM-1-an3	SM-2	SM-2-an1	SM-2-an2	SM-2-an3	SM-3	SM-3-an1	SM-3-an2	SM-3-an3
excitation	$S_0 \rightarrow S_1$	$S_0 \rightarrow S_1$	$S_0 \rightarrow S_1$	$S_0 \rightarrow S_1$	$S_0 \rightarrow S_1$	$S_0 \rightarrow S_1$	$S_0 \rightarrow S_1$	$S_0 \rightarrow S_1$	$S_0 \rightarrow S_1$	$S_0 \rightarrow S_1$	$S_0 \rightarrow S_1$	$S_0 \rightarrow S_1$
E (eV)	3.09	2.71	2.69	2.63	3.17	2.74	2.86	2.63	3.14	2.75	2.82	2.63
D (Å)	1.82	0.932	3.14	6.37	1.95	2.17	3.23	2.39	2.10	2.04	3.68	2.53
E_{Coul} (eV)	2.47	4.48	3.94	2.92	4.51	4.64	3.93	4.37	4.31	4.46	3.77	4.30
S_r	0.68	0.711	0.611	0.494	0.655	0.592	0.626	0.587	0.660	0.633	0.605	0.580
H (Å)	3.69	3.89	3.76	3.77	3.36	2.95	3.73	3.19	3.61	3.32	3.83	3.27
t (Å)	−1.21	−2.07	−0.11	3.09	−0.735	0.101	0.042	0.003	−0.84	−0.656	0.383	0.008
HDI	7.27	7.88	6.74	7.08	8.18	8.42	6.92	8.09	7.81	8.49	6.64	7.99
EDI	7.91	7.74	6.98	8.20	9.44	9.76	8.60	9.84	9.10	9.14	8.92	9.90
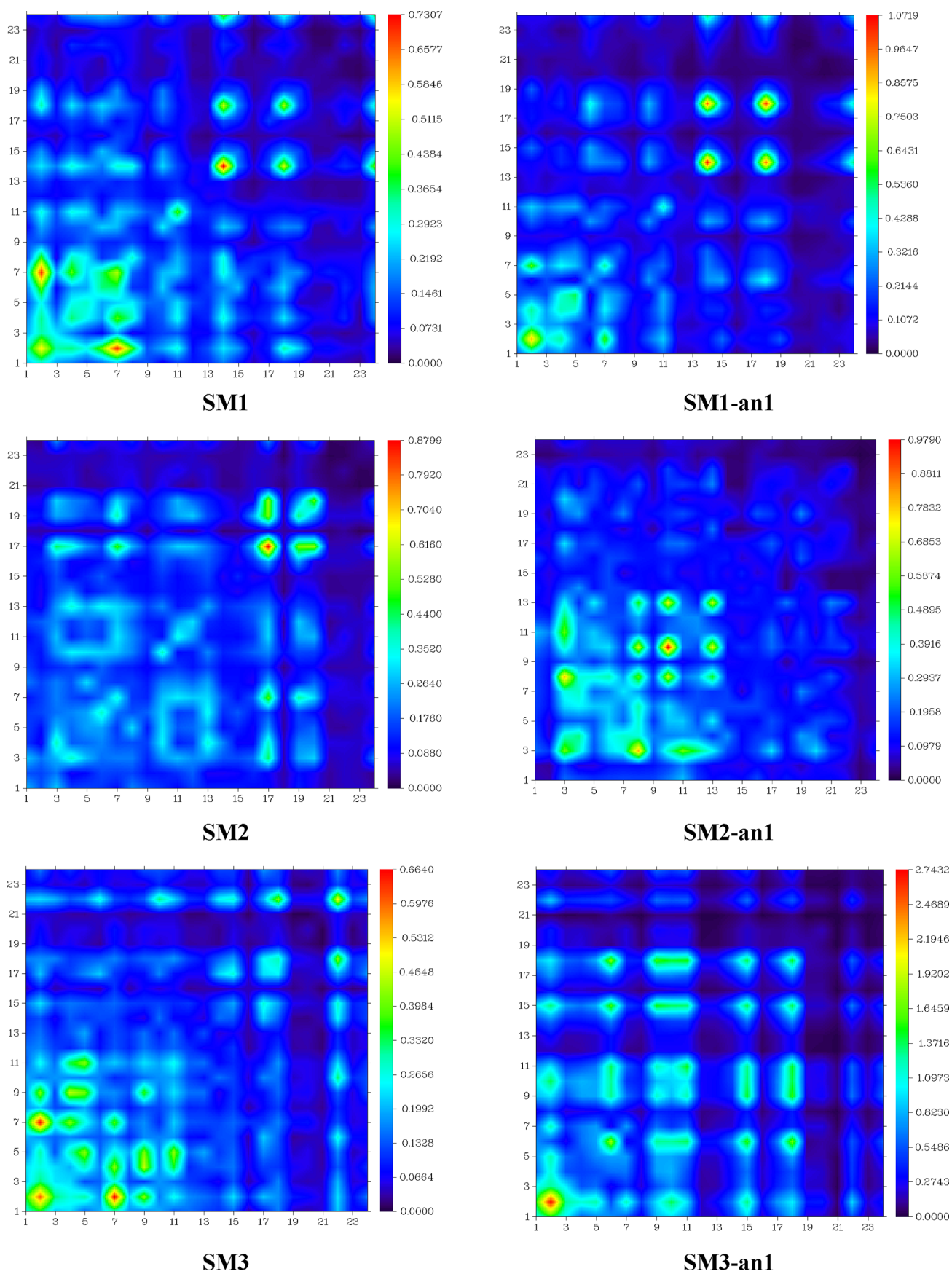
Figure 12. TDM heat map showing the charge transference in sensors and their ions.

4.51 eV among the neutral molecules, but the highest E_{Coul} value is demonstrated by its ion **SM-2-an1** at 4.64 eV. **SM-1** demonstrates the highest S_r index value of 0.68 among all the compounds.

Compounds **SM-1**, **SM-1-an1**, **SM-1-an2**, **SM-2**, **SM-2-an2**, **SM-3**, **SM-3-an1**, and **SM-3-an2** exhibit $\pi-\pi^*$ excitations owing to high S_r index values (>0.6), consequently with high H index values at 3.69, 3.89, 3.76, 3.36, 3.73, 3.61, 3.32, and 3.83 Å, respectively, indicating the presence of extended hole and electron distribution in these compounds. All the neutral compounds exhibit negative t values, indicating main excitation as local excitation (LE) with the ascending order of **SM-1** < **SM-3** < **SM-2**. Relative to their ions, two ions of **SM-1** and only one ion of **SM-3** exhibit a negative t index, i.e., **SM-1-an1** and **SM-1-an2** as well as **SM-3-an1**, respectively, with main excitation being LE in both ions. Finally, the less and similar HDI and EDI values in **SM-1-an1** and **SM-1-an2** also manifest localized excitation. Moreover, the TDM graphs of all the compounds support diagonal charge transference. The charge transfers from nitrogen atoms to oxygen atoms owing to the greater electron-withdrawing capability of the oxygen atom (hydrazine unit). The benzene ring facilitates the charge transfer process from nitrogen toward oxygen as red spots are seen at atoms 15−17. In Figure 12, we showed heat maps of TDM of sensors (**SM-1** to **SM-3**) and their **an1**, while the maps of other ions are shown in Figure S16.

4. CONCLUSIONS

In summary, we have synthesized three sensors, **SM-1** to **SM-3**. These sensors are synthesized in a single step by the condensation of derivative of indole carboxaldehyde with 2,4-dinitrophenyl hydrazine in a good yield. DFT investigations have been also performed for the current study. Efficient charge transference within a molecule from HOMO toward LUMO is investigated through the FMO study. TDM maps further supported this significant transference from indole toward dinitrophenyl hydrazine. Interestingly, it is also investigated that the deprotonated form of sensors is more reactive than their neutral form as lower band gap and greater softness values are found for ions. The UV−vis finding indicated that among all the sensors, **SM-3** showed a wider absorption spectrum. Additionally, the sensor **SM-3** is found as more selective as compared to the other two sensors. **SM-3** displayed high selectivity toward fluoride ions with a low detection limit (8.69×10^{-8}), and the binding constant was determined as 7.7×10^5. The binding mode is proposed as 1:1 stoichiometry based on Job plots. The sensor is successfully used to detect F$^-$ ions in the real sample and used for preparation of strips. We hope that this work will be useful for the design of new sensors for F$^-$ ions.

ASSOCIATED CONTENT

ⓢ Supporting Information

The Supporting Information is available free of charge at https://pubs.acs.org/doi/10.1021/acsomega.3c00821.

> ^{1}H NMR and ^{13}C NMR spectra of **SM-1** to **SM-3**; mixed solution of water/MeCN and **SM-3** without and with addition of F ions; NaF response to **SM-3**; Job plot, B−H plot, and linear plot of **SM-3**; reverse reaction of **SM-3** with water, acids, and other solvents; energy gap of HOMO−1/LUMO+1 and HOMO−2/LUMO+2 of **SM-3**; TDM heat map showing the charge transference in **SM-3** (PDF)

AUTHOR INFORMATION

Corresponding Authors

Rima D. Alharthy − *Department of Chemistry, Science & Arts College, Rabigh Branch, King Abdulaziz University, Rabigh 21911, Saudi Arabia*; Email: iaaalharte@kau.edu.sa

Muhammad Khalid − *Institute of Chemistry and Centre for Theoretical and Computational Research, Khwaja Fareed University of Engineering & Information Technology, Rahim Yar Khan 64200, Pakistan*; Email: khalidhej@hotmail.com, Khalid@iq.usp.br

Zahid Shafiq − *Institute of Chemical Sciences, Bahauddin Zakariya University, Multan 60800, Pakistan*; ⓘ orcid.org/0000-0003-4088-8297; Email: zahidshafiq@bzu.edu.pk

Authors

Nadeem Ahmed − *Institute of Chemical Sciences, Bahauddin Zakariya University, Multan 60800, Pakistan*

Saman Mubarak − *Institute of Chemical Sciences, Bahauddin Zakariya University, Multan 60800, Pakistan*

Muhammad Yaqub − *Institute of Chemical Sciences, Bahauddin Zakariya University, Multan 60800, Pakistan*

Iqra Shafiq − *Institute of Chemistry and Centre for Theoretical and Computational Research, Khwaja Fareed University of Engineering & Information Technology, Rahim Yar Khan 64200, Pakistan*

Muhammad Adnan Asghar − *Department of Chemistry, Division of Science and Technology, University of Education, Lahore 89002, Pakistan*

Ataualpa Albert Carmo Braga − *Departamento de Química Fundamental, Instituto de Química, Universidade de São Paulo, São Paulo 05508-000, Brazil*; ⓘ orcid.org/0000-0001-7392-3701

Complete contact information is available at:
https://pubs.acs.org/10.1021/acsomega.3c00821

Author Contributions

The manuscript was written through the contributions of all authors. All authors have given approval to the final version of the manuscript.

Notes

The authors declare no competing financial interest.

REFERENCES

(1) (a) Carter, K. P.; Young, A. M.; Palmer, A. E. Fluorescent sensors for measuring metal ions in living systems. *Chem. Rev.* **2014**, *114*, 4564−4601. (b) Gale, P. A.; Caltagirone, C. Fluorescent and colorimetric sensors for anionic species. *Coord. Chem. Rev.* **2018**, *354*, 2−27. (c) Suganya, S.; Naha, S.; Velmathi, S. A critical review on colorimetric and fluorescent probes for the sensing of analytes via relay recognition from the year 2012−17. *ChemistrySelect* **2018**, *3*, 7231−7268.

(2) (a) Saleem, T.; Khan, S.; Yaqub, M.; Khalid, M.; Islam, M.; Rehman, M. Y.; Rashid, M.; Shafiq, I.; Braga, A. A.; Syed, A. Novel

quinoline-derived chemosensors: synthesis, anion recognition, spectroscopic, and computational study. *New J. Chem.* **2022**, *46*, 18233−18243. (b) Valeur, B.; Berberan-Santos, M. N. *Molecular fluorescence: principles and applications*; John Wiley & Sons: 2012.

(3) (a) Gale, P. A.; Caltagirone, C. Anion sensing by small molecules and molecular ensembles. *Chem. Soc. Rev.* **2015**, *44*, 4212−4227. (b) HeeáLee, M.; SeungáKim, J. Small molecule-based ratiometric fluorescence probes for cations, anions, and biomolecules. *Chem. Soc. Rev.* **2015**, *44*, 4185−4191.

(4) Kleerekoper, M. The role of fluoride in the prevention of osteoporosis. *Endocrinol. Metab. Clin.* **1998**, *27*, 441−452.

(5) (a) Chen, N.; Zhang, Z.; Feng, C.; Zhu, D.; Yang, Y.; Sugiura, N. Preparation and characterization of porous granular ceramic containing dispersed aluminum and iron oxides as adsorbents for fluoride removal from aqueous solution. *J. Hazard. Mater.* **2011**, *186*, 863−868. (b) Organization, W. H *Boron in drinking-water: Background document for development of WHO Guidelines for Drinking-water Quality*; World Health Organization: 2009; (c) Xiong, X.; Liu, J.; He, W.; Xia, T.; He, P.; Chen, X.; Yang, K.; Wang, A. Dose−effect relationship between drinking water fluoride levels and damage to liver and kidney functions in children. *Environ. Res.* **2007**, *103*, 112−116.

(6) (a) Jung, H. S.; Kim, H. J.; Vicens, J.; Kim, J. S. A new fluorescent chemosensor for F− based on inhibition of excited-state intramolecular proton transfer. *Tetrahedron Lett.* **2009**, *50*, 983−987. (b) Li, J.; Lin, H.; Cai, Z.; Lin, H. A high selective anion colorimetric sensor based on salicylaldehyde for fluoride in aqueous media. *Spectrochim. Acta, Part A* **2009**, *72*, 1062−1065. (c) Lin, T.-P.; Chen, C.-Y.; Wen, Y.-S.; Sun, S.-S. Synthesis, photophysical, and anion-sensing properties of quinoxalinebis (sulfonamide) functionalized receptors and their metal complexes. *Inorg. Chem.* **2007**, *46*, 9201−9212. (d) Palacios, M. A.; Wang, Z.; Montes, V. A.; Zyryanov, G. V.; Hausch, B. J.; Jursíková, K.; Anzenbacher, P., Jr. Hydroxyquinolines with extended fluorophores: arrays for turn-on and ratiometric sensing of cations. *Chem. Commun.* **2007**, *36*, 3708−3710. (e) Zhang, J. F.; Lim, C. S.; Bhuniya, S.; Cho, B. R.; Kim, J. S. A highly selective colorimetric and ratiometric two-photon fluorescent probe for fluoride ion detection. *Org. Lett.* **2011**, *13*, 1190−1193.

(7) Snowden, T. S.; Anslyn, E. V. Anion recognition: synthetic receptors for anions and their application in sensors. *Curr. Opin. Chem. Biol.* **1999**, *3*, 740−746.

(8) Cametti, M.; Rissanen, K. Recognition and sensing of fluoride anion. *Chem. Commun.* **2009**, *20*, 2809−2829.

(9) (a) Anzenbacher, P.; Jursíková, K.; Sessler, J. L. Second generation calixpyrrole anion sensors. *J. Am. Chem. Soc.* **2000**, *122*, 9350−9351. (b) Chellappan, K.; Singh, N. J.; Hwang, I. C.; Lee, J. W.; Kim, K. S. A calix [4] imidazolium [2] pyridine as an anion receptor. *Am. Ethnol.* **2005**, *117*, 2959−2963. (c) Descalzo, A. B.; Rurack, K.; Weisshoff, H.; Martínez-Máñez, R.; Marcos, M. D.; Amorós, P.; Hoffmann, K.; Soto, J. Rational design of a chromo-and fluorogenic hybrid chemosensor material for the detection of long-chain carboxylates. *J. Am. Chem. Soc.* **2005**, *127*, 184−200. (d) Devaraj, S.; Saravanakumar, D.; Kandaswamy, M. Dual chemosensing properties of new anthraquinone-based receptors toward fluoride ions. *Tetrahedron Lett.* **2007**, *48*, 3077−3081. (e) Jose, D. A.; Kar, P.; Koley, D.; Ganguly, B.; Thiel, W.; Ghosh, H. N.; Das, A. Phenol-and catechol-based ruthenium (II) polypyridyl complexes as colorimetric sensors for fluoride ions. *Inorg. Chem.* **2007**, *46*, 5576−5584. (f) Jose, D. A.; Kumar, D. K.; Ganguly, B.; Das, A. Urea and thiourea based efficient colorimetric sensors for oxyanions. *Tetrahedron Lett.* **2005**, *46*, 5343−5346. (g) Lin, C.-I.; Selvi, S.; Fang, J.-M.; Chou, P.-T.; Lai, C.-H.; Cheng, Y.-M. Pyreno [2, 1-b] pyrrole and bis (pyreno [2, 1-b] pyrrole) as selective chemosensors of fluoride ion: a mechanistic study. *J. Org. Chem.* **2007**, *72*, 3537−3542. (h) Liu, B.; Tian, H. A ratiometric fluorescent chemosensor for fluoride ions based on a proton transfer signaling mechanism. *J. Mater. Chem.* **2005**, *15*, 2681−2686. (i) Qiao, Y.-H.; Lin, H.; Lin, H.-K. A novel colorimetric sensor for anions recognition based on disubstituted phenylhydrazone. *J. Inclusion Phenom. Macrocyclic Chem.* **2007**, *59*, 211−215. (j) Zhang,

X.; Guo, L.; Wu, F.-Y.; Jiang, Y.-B. Development of fluorescent sensing of anions under excited-state intermolecular proton transfer signaling mechanism. *Org. Lett.* **2003**, *5*, 2667−2670.

(10) (a) Dong, Z. M.; Wang, W.; Wang, Y. B.; Wang, J. N.; Qin, L. Y.; Wang, Y. A reversible colorimetric chemosensor for "Naked Eye" sensing of cyanide ion in semi-aqueous solution. *Inorg. Chim. Acta* **2017**, *461*, 8−14. (b) Gupta, V. K.; Singh, A. K.; Bhardwaj, S.; Bandi, K. R. Biological active novel 2, 4-dinitro phenyl hydrazones as the colorimetric sensors for selective detection of acetate ion. *Sens. Actuators, B* **2014**, *197*, 264−273. (c) Kodlady, S. N.; Narayana, B.; Sarojini, B.; Gauthama, B. Aromatic aldehyde based chemosensors for fluoride and cyanide detection in organic and aqueous media: ascertained by characterization, spectroscopic and DFT studies. *Inorg. Chim. Acta* **2019**, *494*, 245−255. (d) Tanwar, S.; Lu, H.-Y.; Magi, E.; Ho, J.-a. A. A 2, 4-dinitrophenylhydrazine/kojic acid derivative as a simple colorimetric probe for determination of cupric ions in water. *Sens. Actuators, B* **2014**, *203*, 204−208.

(11) Carlsen, R.; Jenkins, J. R.; Ess, D. H. Direct dynamics analysis of the cationic Cp*(PMe 3) Ir (CH 3) methane C−H activation mechanism. *Faraday Discuss.* **2019**, *220*, 414−424.

(12) Lemke, K. H.; Seward, T. M. Thermodynamic properties of carbon dioxide clusters by M06-2X and dispersion-corrected B2PLYP-D theory. *Chem. Phys. Lett.* **2013**, *573*, 19−23.

(13) (a) Ahmed, N.; Zareen, W.; Shafiq, Z.; de Alcântara Morais, S. F.; Khalid, M.; Braga, A. A. C.; Munawar, K. S.; Yong, Y. A coumarin based Schiff Base: An effective colorimetric sensor for selective detection of F−ion in real samples and DFT studies. *Spectrochim. Acta, Part A* **2023**, *286*, No. 121964. (b) Arooj, M.; Zahra, M.; Islam, M.; Ahmed, N.; Waseem, A.; Shafiq, Z. Coumarin based thiosemicarbazones as effective chemosensors for fluoride ion detection. *Spectrochim. Acta, Part A* **2021**, *261*, No. 120011.

(14) Basri, R.; Ahmed, N.; Khalid, M.; Khan, M. U.; Abdullah, M.; Syed, A.; Elgorban, A. M.; Al-Rejaie, S. S.; Braga, A. A. C.; Shafiq, Z. Quinoline based thiosemicarbazones as colorimetric chemosensors for fluoride and cyanide ions and DFT studies. *Sci. Rep.* **2022**, *12*, 4927.

(15) Zhou, Y.; Bao, X. Synthesis, recognition and sensing properties of dipyrrolylmethane-based anion receptors. *Spectrochim. Acta, Part A* **2019**, *210*, 1−8.

(16) Isaac, I. O.; Munir, I.; Al-Rashida, M.; Ali, S. A.; Shafiq, Z.; Islam, M.; Ludwig, R.; Ayub, K.; Khan, K. M.; Hameed, A. Novel acridine-based thiosemicarbazones as 'turn-on'chemosensors for selective recognition of fluoride anion: a spectroscopic and theoretical study. *R. Soc. Open Sci.* **2018**, *5*, No. 180646.

(17) Pangannaya, S.; Trivedi, D. R. Electrooptical characteristics and anion binding behaviour of organic receptors: Effect of substitution on colorimetric response. *Sens. Actuators, B* **2017**, *247*, 673−680.

(18) Janeková, H.; Gašpar, J.; Gáplovský, A.; Stankovičová, H. Selective fluoride chemosensors based on coumarin semicarbazones. *J. Photochem. Photobiol., A* **2021**, *410*, No. 113168.

(19) Uzun, S.; Esen, Z.; Koç, E.; Usta, N. C.; Ceylan, M. Experimental and density functional theory (MEP, FMO, NLO, Fukui functions) and antibacterial activity studies on 2-amino-4-(4-nitrophenyl)-5, 6-dihydrobenzo [h] quinoline-3-carbonitrile. *J. Mol. Struct.* **2019**, *1178*, 450−457.

(20) Gefen, A. *Innovations and Emerging Technologies in Wound Care*; Academic Press, 2019.

(21) (a) Parr, R. G.; Yang, W. Density functional approach to the frontier-electron theory of chemical reactivity. *J. Am. Chem. Soc.* **1984**, *106*, 4049−4050. (b) Kamat, V.; Kumara, K.; Naik, K.; Kotian, A.; Netalkar, P.; Shivalingegowda, N.; Neratur, K. L.; Revankar, V. [Dichlorido (2-(2-(1H-benzo[d]thiazol-2-yl)hydrazono)propan-1-ol) Cu(II)]: Crystal structure, Hirshfeld surface analysis and correlation of its ESI-MS behavior with [Dichlorido 3-(hydroxyimino)-2-butanone-2-(1H-benzo[d]thiazol-2-yl)hydrazone Cu(II)]. *J. Mol. Struct.* **2017**, *1149*, 357e366. (c) Tarı, G. Ö.; Ceylan, Ü.; Ağar, E.; Eserci, H. Crystal structure, spectroscopic investigations and quantum chemical computational study of 5-(diethylamino)-2-((3-nitropheny-limino) methyl) phenol. *J. Mol. Struct.* **2016**, *1126*, 83−93.

(22) Vinutha, M.; Venkatesha, T. Review on mechanistic action of inhibitors on steel corrosion in acidic media. *Port. Electrochim. Acta* **2016**, *34*, 157−184.

(23) (a) Chattaraj, P. K.; Roy, D. R. Update 1 of: electrophilicity index. *Chem. Rev.* **2007**, *107*, PR46-PR74. (b) Lesar, A.; Milošev, I. Density functional study of the corrosion inhibition properties of 1, 2, 4-triazole and its amino derivatives. *Chem. Phys. Lett.* **2009**, *483*, 198−203. (c) Parr, R. G.; Szentpály, L.; Liu, S. Electrophilicity index. *J. Am. Chem. Soc.* **1999**, *121*, 1922−1924.

(24) (a) Mazhar, S.; Khalid, M.; Tahir, M. N.; Haroon, M.; Akhtar, T.; Khan, M. U.; Jaleel, F.; Aslam, M. Facile Synthesis, Crystal Growth, Quantum Chemical Studies of Electronic Structure and of the Profoundly Persuasive NLO Organic Crystal: Ethyl 4-[N, N-bis (p-toluenesulfonyl)]-Aminobenzoate. *J. Chem. Soc. Pak.* **2019**, *41*, 122−122. (b) Vijayaraj, R.; Subramanian, V.; Chattaraj, P. Comparison of global reactivity descriptors calculated using various density functionals: a QSAR perspective. *J. Chem. Theory Comput.* **2009**, *5*, 2744−2753.

(25) (a) Chattaraj, P.; Nath, S.; Maiti, B. *Reactivity descriptors*; Marcel Dekker: New York: 2003; (b) Koopmans, T. Ordering of wave functions and eigenenergies to the individual electrons of an atom. *Physica* **1934**, *1*, 104−113. (c) Parr, R. G.; Chattaraj, P. K. Principle of maximum hardness. *J. Am. Chem. Soc.* **1991**, *113*, 1854−1855. (d) Pearson, R. G. Absolute electronegativity and absolute hardness of Lewis acids and bases. *J. Am. Chem. Soc.* **1985**, *107*, 6801−6806.